ORIGINAL ARTICLE

Depth of the pedological profile as a conditioning factor of soil erodibility (RUSLE K-Factor) in Ecuadorian basins

Daniel Delgado[1,2] · Mahrez Sadaoui[1] · Wolfgang Ludwig[1] · Williams Mendez[2]

Abstract

Soil erodibility (K-Factor) is one of the fundamental parameters to estimate its rainfall erosion through mathematical models such as RUSLE. Carrying out an erodibility analysis at different pedological depths allows identifying what would be its susceptibility to erosion processes. Soil unit parcel data obtained by long-term field measurements are required, ensuring that the analyzed sections remain uncovered throughout observation period, investing large amounts of time and money. However, the lack of a good and extensive field database is the main limitation to apply this methodology. The objective of this work was to analyze the spatial distribution of soil erodibility in different pedological profiles, through the implementation of satellite data of soil characteristics. The methodology consisted in delimiting and analyzing the environmental characteristics of the Ecuadorian basins, obtaining the clay, silt, sand SOC contents of the analyzed depths, determining the K-Factor values and comparing them with environmental layers. Basins delimitation and environmental characteristics were extracted from regional literature; soil layer contents were obtained from SoilGrids; K-Factor calculation was made from soil characteristics using Software R and QGIS; results comparison against the elevation and land cover parameters were carried out using QGIS. The results allowed to identify very small variations between pedological profiles; determine that clay and silt are the most incident elements of K-Factor; identify that Crop and Grass are coverages that concentrate on the highest values of K-Factor as well as the highest areas. This allows the administrators of the territory to generate measures to reduce soil loss.

Keywords Soil erosion · RUSLE · Soil erodibility · Erodibility factor · K-Factor

Introduction

Erosion is considered one of the main causes of soil degradation worldwide (Prasannakumar et al. 2011; Amundson et al. 2015; Bastola et al. 2018). This process, in addition to generating infertility and reducing crop yields (Tang et al. 2021), is one of the main causes of eco-environmental problems, among which scenarios of socio-natural disasters stand out (processes of removal of masses), solid load in pluvial transport, water pollution, among others (Wang et al. 2017). The processes associated with erosion (such as landslides), the mobilization and deposition of organic and mineral particles from the soil together with their associated contaminants (heavy metals, among others) frequently cause the contamination of water bodies, affecting their storage quality, use efficiency and shelf life (Wei et al. 2019). Anthropogenic actions, such as deforestation and agricultural expansion, added to extreme weather events, have significantly accelerated erosion processes and their devastating consequences worldwide (Yin et al. 2018).

Ecuador is considered the country with the highest deforestation rate in South America, which generates large-scale soil erosion problems (Ochoa-Cueva et al. 2013). Between 2010 and 2020, an average forest loss of 53,000 ha/year has been recorded throughout the Ecuadorian territory (FAO 2020) and, even though these statistics have decreased compared to the previous period (2000–2010, 70,200 ha/year /year), continues to be a threat that contributes to the soil loss intensification due to water

✉ Daniel Delgado
  daniel.delgado@utm.edu.ec

[1] Centre de Formation et de Recherche sur les Environnements Méditerranéens, Université de Perpignan, Via Domitia, UMR 5110, 52 Avenue Paul Alduy, 66860 Perpignan CEDEX, France

[2] Departamento de Construcciones Civiles, Facultad de Ciencias Matemáticas, Físicas y Químicas, Universidad Técnica de Manabí, Avenida José María Urbina, Portoviejo EC130105, Manabí, Ecuador

erosion in the country. Despite this, studies related to soil erosion in Ecuador are very scarce, limited to the analysis of coastal subregions (Pacheco et al. 2019), sectors of the Andean Mountain (Ochoa-Cueva et al. 2013; Ochoa et al. al. 2016) or to individual conditioning factors that have not considered the soil erodibility (Delgado et al. 2021, 2022). This could mask the real magnitude of the triggers and the effects linked to the soil loss in Ecuador.

To estimate soil erosion, it is possible to use mathematical models that employ theoretical, empirical, conceptual and physical processes (Rehman et al. 2022). Among the most widely used models are the Universal Soil Loss Equation (USLE) (Wischmeier and Smith 1978) and its revised version, RUSLE (Renard et al. 1996). Both methodologies use the same factors to estimate soil erosion: 1) R-Factor (rainfall erosivity, main erosion trigger, Delgado et al. 2022); 2) K-Factor (soil erodibility; 3, 4) LS-Factor (topographic factor resulting from the combination of the length and slope of the land); C-Factor (management and land cover) and; 6) P-Factor (soil conservation practices).

Within these components, soil erodibility (K-Factor) determines its resistance to withstand erosion (Musa et al. 2017), and indicates the degree of difficulty with which it is disaggregated, eroded and with which the particles are set in motion by the impact of raindrops (R-Factor) and surface runoff (Wishmeier and Mannering 1969). This complex factor is affected by other processes and conditions, among which rainfall, surface runoff, soil infiltration, aggregate stability, shear strength, terrain type, vegetation and land use stand out (Bonilla and Johnson 2012).

K-Factor analysis has been restricted almost exclusively to topsoil without considering other levels (depths) of its pedological profile that may be exposed or be completely dragged, because of mass soil removal processes (landslides), exposing, in many cases, the parent material. This methodological routine limits the possibility of a more soil erodibility exhaustive analysis, in which the behavior and contribution of its conditioning elements are considered, depending on the depth.

Generally, K-Factor is determined by long-term measurements of unitary erosion plots, at a length of 22.1 m and a slope of 9%, considering that these sections must remain uncovered throughout the observation period (Wischmeier and Smith 1978). This methodology generates much more precise values. However, this procedure requires elaborate facilities and long observation periods, generating high economic costs and exhaustive study seasons (Rehman et al. 2022). Cassol et al. (2018) consider that field studies should have a minimum duration of 10 years of observation and data collection to reliably estimate soil erodibility results. Otherwise, a short-term analysis would generate underestimates in K-Factor magnitudes.

In much of the world, and especially in Ecuador, the lack of a dense and extensive soil erodibility database (obtained in field) is a major limitation for the application and development of this methodology. However, there are currently many studies that have determined the K-Factor from satellite information, with experiences developed in Africa (Mhangara et al. 2012; Elnashar et al. 2021), Europe (Gürtekin and Gökçe 2021), Asia (Saha et al. 2022), Oceania (Yang et al. 2022a, b), and even South America (Riquetti et al. 2022). The accessibility restrictions or the absence of field information and the new methodologies applied have allowed us to reflect on the search for other alternatives and data types, so in this investigation satellite images were used to estimate K-Factor a level of Ecuadorian continental territory.

Currently, there are several sources that allow free and almost global soil profile data to be obtained, including GlobalSoilMaps from the Natural Resources Conservation Service Soils (USDA) and SoilGrids from the World Soil Information (ISRIC). SoilGrids database has been applied and validated in many previous investigations worldwide (Krpec et al. 2020; Bahri et al. 2022; Huang et al. 2022), which have yielded very reliable results.

Among the main advantages of using SoilGrids, its high spatial resolution and smaller mean errors stand out in relation to other satellite databases; however, it has a limitation of overestimating carbon content, having restricted soil fractions and presenting uncertainties (especially in its vertical resolution). These conditions, together with free access to its database and the availability of information at various soil profile depths, allow SoilGrids to be classified as a reliable and ideal database to be used in the context of Ecuadorian territory.

The main objective of this research is to analyze how the depth of the pedological profile conditions the soil erodibility in Ecuadorian basins, both for Ecuadorian Coastal Basins (ECBs) that flow into the Pacific Ocean, and for Amazon Tributaries Basins (ATBs). This paper analyzes the contribution (variability) and behavior of the soil elements (texture and soil organic carbon "SOC") that determine its erodibility, depending on the depth of the pedological profile, both in ECBs and ATBs. For this, it was necessary to demarcate, in the first place, basins of Ecuadorian territory with surfaces greater than 500 km^2. Likewise, data (soil texture and SOC) were collected from the soil profile at different depths (0–30 cm "topsoil"; 30–60 cm and; 100–200 cm) in each basin of study area; and the projection (WGS84-UTM zone 17S) and spatial resolution (fine resolution, 100×100 m) of the raster information collected for the study were homogenized.

Results of this work will allow interpreting the soil erodibility as the variability and contribution of its conditioning components in the national territory, depending on the

depth. This represents a contribution with a positive impact for a better approximation in soil erosion estimation rates through RUSLE, which will contribute to environmental planning focused on the execution of soil conservation practices, and the promotion of its sustainable use.

Study area

The research has been developed in the continental territory of Ecuador, in South America, bounded to the north by Colombia, to the south and east by Peru, and to the west by the Pacific Ocean. Due to its geographical location, Ecuadorian continental territory is divided into 3 regions: Coast, Andes/Sierra and Amazon (Fig. 1).

Basins delimitation was determined through Delgado et al. (2021) and was adjusted to a spatial resolution of 100×100 m (initial resolution of 4×4 km). The 32 basins were obtained by considering only areas greater than 500 km^2, identifying dimensions from 542 km^2 (Id 11 in Fig. 1 and Supplementary data, Ayampe) to 38,000 km^2 (Id 31 in Fig. 1 and Supplementary data, Napo), covering approximately 80% of the Ecuadorian territory (227,000 km^2).

The 24 basins that are distributed to the west of the Andes Mountain are called ECBs, which discharge into the Pacific Ocean. Within these ECBs, 3 basins stand out that are represented in pink, due to the particularity of discharging also within the Pacific Ocean, but outside Ecuadorian territory (Id 1 in Colombia; Id 23 and 24 in Peru, Fig. 1).

The 8 basins that are located to the East of the Andes Mountain are called ATBs, which discharge into the Amazon. These basins have different characteristics and, in addition to having much larger areas on average in relation to ECBs, they also present special weather conditions that generate a record of constant rainfall throughout the year (Delgado et al. 2022).

Materials and methods

Ecuadorian basins characteristics

Elevation (m) and Land Cover were also extracted and processed from Delgado et al, (2021). Spatial resolutions were converted to a common grid point of 100 m.

Figure 2a shows that the presence of the Andes Mountains generates a particular distribution of altitudes, in
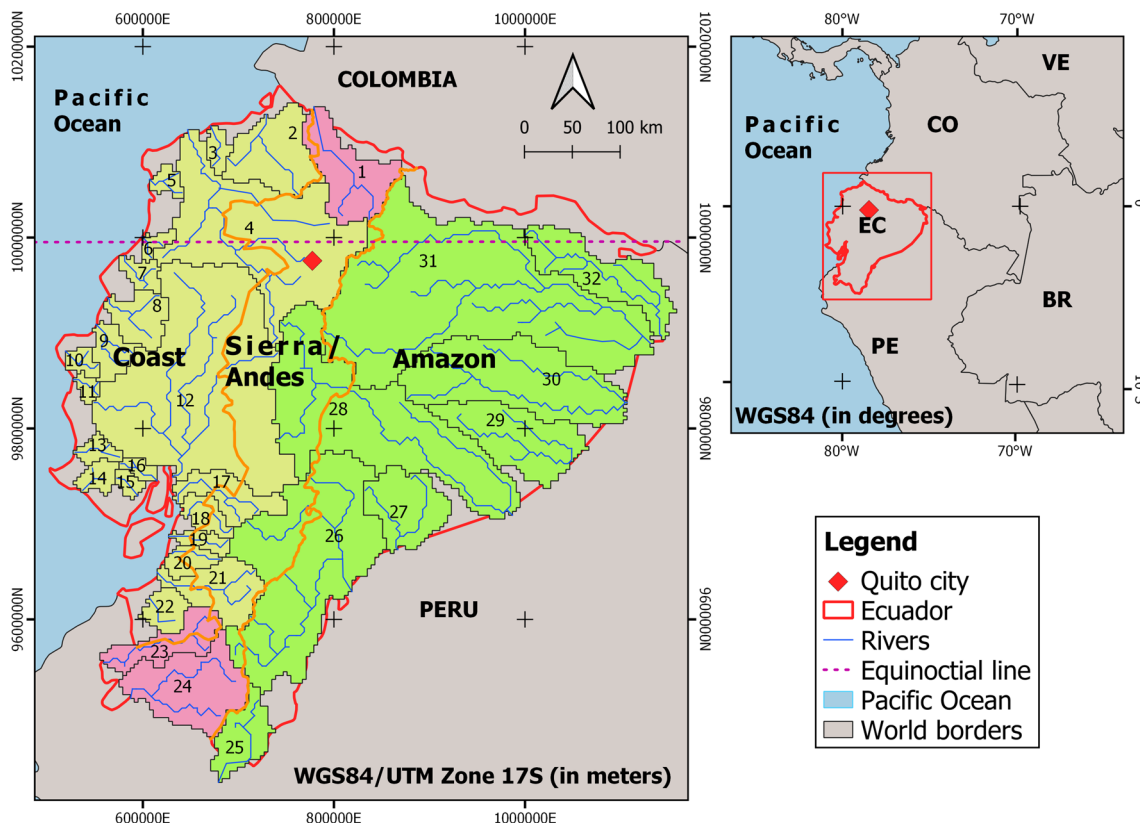

Fig. 1 Map of the study area and basins distribution in Ecuadorian territory (32 basins). Yellow and pink colors represent ECBs and green colors ATBs. Numbering shows the assignment ID for each basin
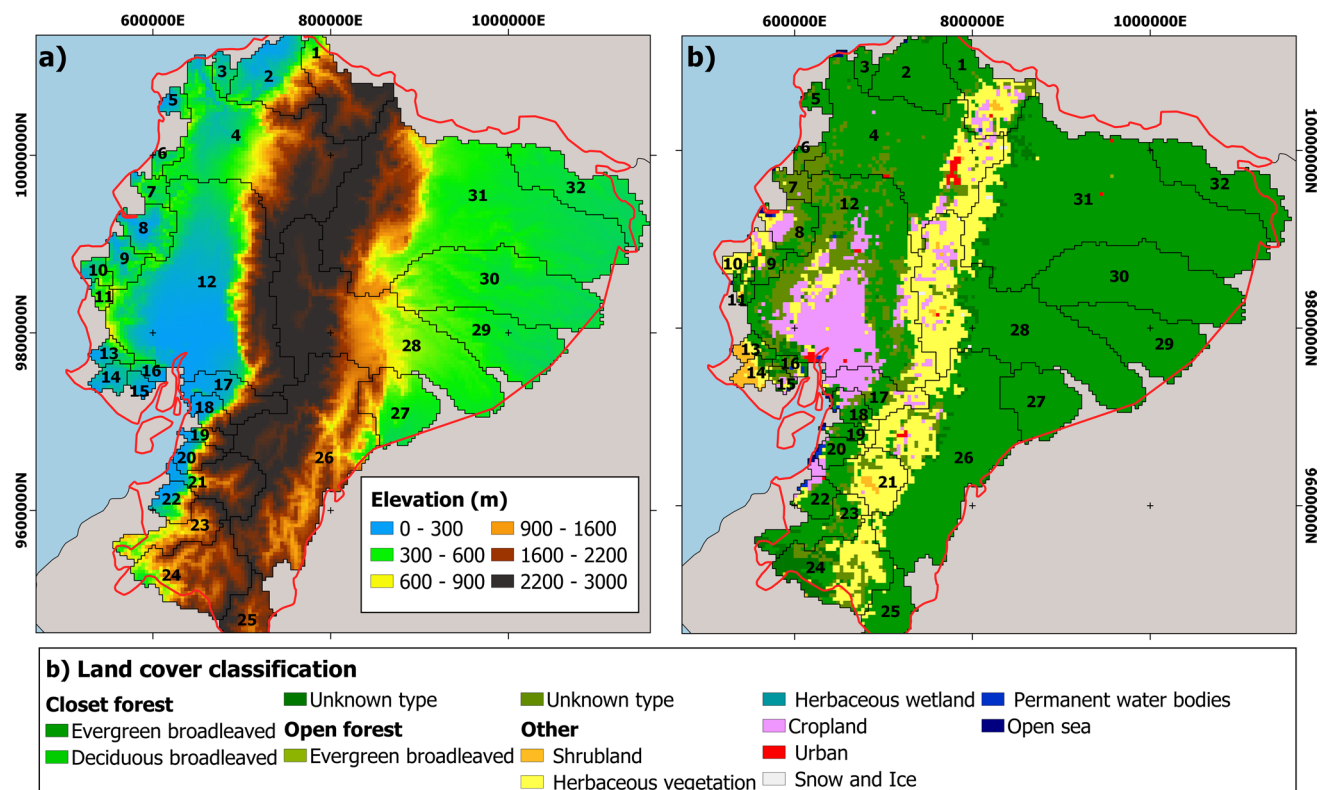
Fig. 2 Ecuadorian basins spatial environmental characteristics. **a** Elevation; **b** Land cover classification

addition to being considered a dividing barrier between the Coast and Amazon regions (Delgado et al. 2022). This mountain registers the highest elevations in Ecuadorian territory, so that sectors of the basins that are close to it present heights per pixel greater than 5000 m, both in ECBs and ATBs, while the minimum values are below 1 m and are in the discharge areas of ECBs to Pacific. With respect to the range of average elevations by basins, values oscillate between 2200 m in the ECB Mira (Id 1 in Fig. 2a and Supplementary data) and 60 m in ECB Daule (Id 15 in Fig. 2a and Supplementary data). On average, ATBs have higher elevations, with 1048 m compared to 722 m for ECBs.

Regarding Land Cover (Fig. 2b), 13 classes were identified and classified into 3 groups: open forests (discontinuous set of trees that represent between 10 and 40% of the area), closed forests (continuous set of trees that represent more than 40% of the area) and others. It was determined that forests cover 84% of study area (60% closed forests and 24% open forests). Forests, in turn, register a higher concentration of ATBs. In "other" classification, herbaceous vegetation and cropland stand out, representing 59% and 21% of this group, respectively. Cropland zones predominated within ECBs Taura and Guayas (Id 17 and 12 in Fig. 2b, respectively), reaching 39% and 28% of their extension areas.

Soil textures and SOC compilation

Grid-level soil information was obtained from SoilGrids (ISRIC, https://soilgrids.org/). This database provides a global digital soils mapping using machine learning methodologies that generate more than 230,000 soil profile observations worldwide, in addition to a series of measurements of environmental covariates (climate, land cover, soil morphology).

The spatial resolution is 250 m and they have the following soil properties: pH, SOC content, bulk density, coarse fragment, sand, silt and clay content, cation exchange capacity, nitrogen total and SOC density. Almost all these properties are available in the following depths: (1) 0–5 cm; (2) 5–15 cm; (3) 15–30 cm; (4) 30–60 cm; (5) 60–100 cm; (6) 100–200 cm.

For the present investigation, physical properties of Clay (g/kg), Sand (g/kg) and Silt (g/kg) were considered. SOC (dg/kg) was considered as a soil chemical property. To determine the role played by the depth of the soil's pedological profile as determinants of its erosion, the following depths were analyzed: (1) 0–5 cm; (2) 30–60 cm and; (3) 100–200 cm.

Eleven $2 \times 2°$ mosaics (approximately 200×200 km) were downloaded to cover the entire Ecuadorian territory, starting from latitudes 6°S and 2°N and longitudes 81°W and 77°S. To

adapt information obtained from SoilGrids, data were homogenized with WGS84-UTM zone 17S projection and spatial resolution was improved to 100×100 m using Software R (with RStudio complement) and QGIS, so that the current model allows a coupling with data of different spatial resolutions (especially with higher resolutions) when using K-Factor as an element to determine soil erosion through RUSLE.

RUSLE K-factor calculation

RUSLE is the most widely used soil loss estimation model in many regions of the world (Delgado et al. 2022). K-Factor calculates the soil resistance against the rainfall erosive force and the runoff energy.

Soil erodibility estimation depends on its properties such as particle size, organic matter content, structure and permeability. Soil erodibility are calculated in a range of 0.05–0.69 (Al Rammahi and Khassaf 2018). High clay soils generate low K-Factor values, generally in ranges from 0.05 to 0.15, as well as a coarse-textured sandy soil (0.05 to 0.20), due to the resistance of these soils to detachment (Goldman and Jackson 1986).

Within the K-Factor calculation, the soil erodibility main factor is the percentage silt content that represents the total content of topsoil, because silt easily detaches forming crusts that allow high runoff rates to be produced (Al Rammahi and Khassaf 2018). This is the reason why soils that have had a high silt content are the most erodible in relation to other types.

SOC is also considered in K-Factor calculation thanks to its effect on soil erosion. This particular content lowers erodibility values, reducing susceptibility to soil erosion by increasing water infiltration rates through soil layers (a high-water infiltration rate decrease runoff).

Williams equation (Williams 1995; Neitsch et al. 2000) was used to determine the soil erodibility (Eq. 1):

$$K_{usle} = f_{csand} \times f_{cl-si} \times f_{orgc} \times f_{hisand,} \tag{1}$$

where, K_{usle}: USLE model soil erodibility factor.f_{csand}: factor that lowers the K-Factor indicator in soils with high content of coarse sand and increases it for soils with little sandf_{cl-si}: low K-Factor values for soils with high clay to silt ratiosf_{orgc}: reduces K-Factor values in soils with high SOCf_{hisand}: lowers K-Factor values for soils with extremely high sand content

Initially, this equation was generated to be applied in the USLE methodology. To apply it in the RUSLE, it is enough to convert the results to the International System, using a conversion factor of 0.1317 (Al Rammahi and Khassaf 2018) (Eq. 2):

$$K_{Rusle} = K_{usle} \times 0.1317, \tag{2}$$

where K_{Rusle}: soil erodibility factor adapted for RUSLE (t h/MJ mm).

Complementary K-Factor elements are detailed below (Eqs. 3, 4, 5 and 6):

$$f_{csand} = \left\{ 0.2 + 0.3 \times \exp\left[-0.256 \times m_s \times \left(1 - \frac{m_{silt}}{100} \right) \right] \right\}, \tag{3}$$

$$f_{cl-si} = \left(\frac{m_{silt}}{m_c + m_{silt}} \right)^{0.3}, \tag{4}$$

$$f_{orgc} = \left\{ 1 - \frac{0.25 \times orgC}{orgC + \exp(3.75 - 2.95 \times orgC)} \right\}, \tag{5}$$

$$f_{hisand} = \left\{ 1 - \frac{0.7 \times \left(1 - \frac{m_s}{100} \right)}{\left(1 - \frac{m_s}{100} \right) + \exp\left[-5.51 + 22.9 \times \left(1 - \frac{m_s}{100} \right) \right]} \right\}, \tag{6}$$

where m_s: percentage of sand fraction content (0.50–2.00 mm diameter of particles). m_{silt}: percentage of silt fraction content (0.002–0.05 mm particle diameter). m_c: clay fraction content percentage (greater than 0.002 mm particle diameter). orgC: percentage of SOC fraction.

To use Eq. 2, it was necessary to convert the layers to percentages for each pixel under study. This procedure consisted of adding the amount of the 4 soil elements analyzed (clay, sand, silt and SOC) to subsequently identify the percentage representation of each of them. Because SOC layer had different units than those shown in the 3 soil textures, it was necessary to first convert it from hg/kg to g/kg, applying a conversion factor of SOC/10. Additionally, because certain sectors of Ecuadorian basins registered values of 0, when applying Eq. 2, sub-areas with lack of data were generated, for which a data filling procedure was carried out. This procedure consisted of filling raster regions with no-data values by interpolating from the edges, using the QGIS "Fill nodata" command (allows the values of the regions with no-data to be calculated by the surrounding pixel values using inverse distance weighting). Methodological summary of the research can be seen in Fig. 3.

Results

Soil properties

Clay content

Figure 4a shows clay content found in topsoil and the soil part that would be directly affected by R-Factor. At pixel level, clay content values ranged from 0 to 572 g/kg, with higher concentrations in the Northeast of the country, in ATBs. Within the ECBs clay contents did not exceed 450 g/
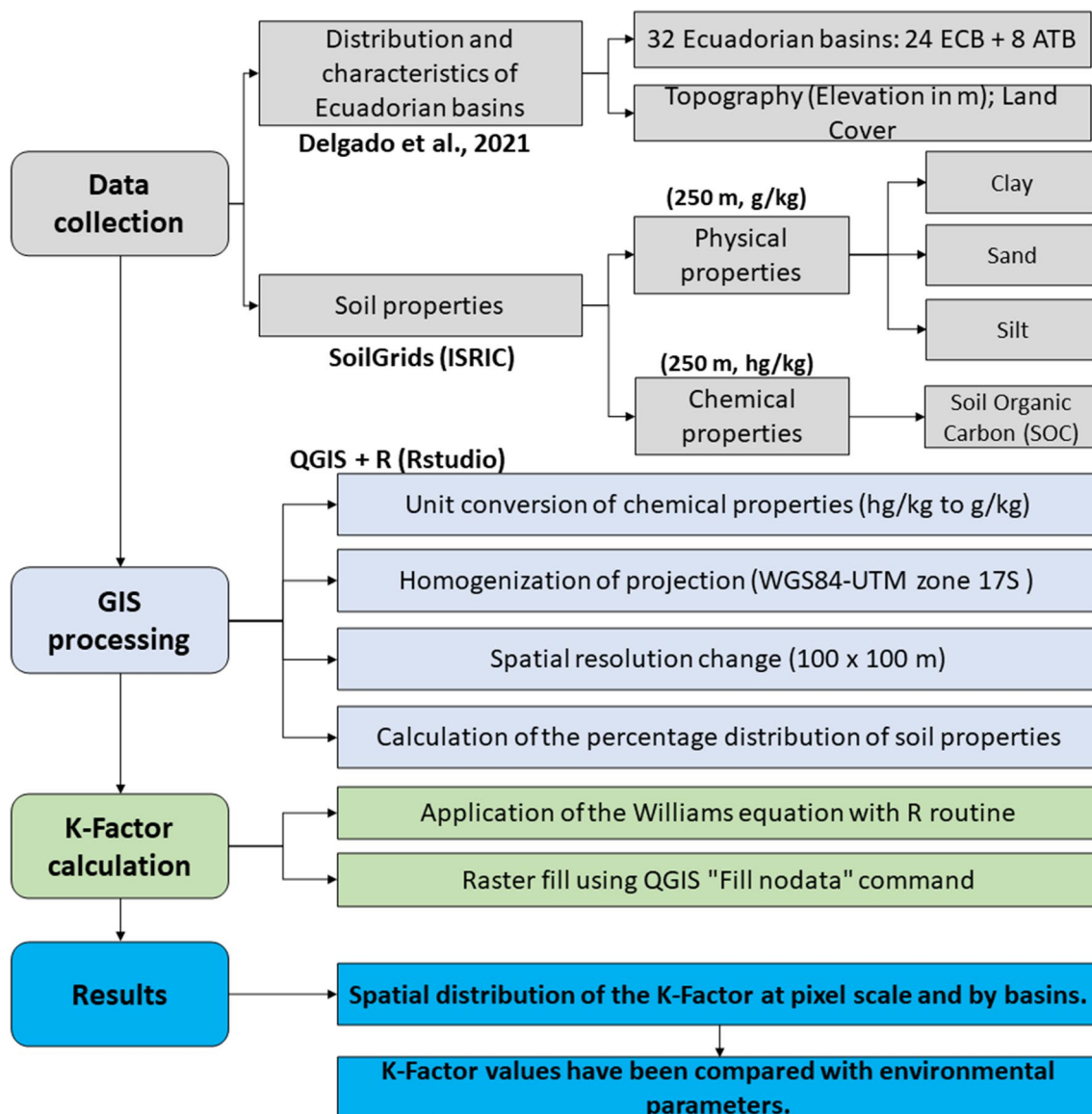
Fig. 3 Flowchart shows methodology applied in this study to calculate K-Factor

kg. The average value at the national level was 307.51 g/kg. At basins level, ATB Conocoto-Curaray (Id 30 in Fig. 4a and Supplementary data) is the one that registers the highest amount of clay, reaching 377.26 g/kg, while ECB Jubones (Id 21 in Fig. 4a and Supplementary data) is the one that registers the least amount of clay, with 254.11 g/kg (approximately 33% less clay in relation to ATB).

Analyzing Fig. 4b, which represents the clay content at a depth of 30–60 cm, a higher concentration of this soil type can be observed in this layer in relation to topsoil (16% more on average). Clay concentrations spatial distribution maintains great similarity with topsoil, but values higher than 500 g/kg are already recorded in certain ECBs at pixel level, especially in ECB Guayas (Id 12 in Fig. 4b, Supplementary

data). At this same level, clay was recorded from 0 to 747 g/kg, with an average value of 355.07 g/kg. At basins level, the distribution of the maximum and minimum values is maintained in relation to topsoil, registering the highest values in the ATB Conocoto-Curaray (Id 30 in Fig. 4b and Supplementary data) with 451.33 g/kg and the lowest values were recorded in Jubones ECB (Id 21 in Fig. 4b and Supplementary data) with 281.48 g/kg (approximately 38% less in relation to ECB).

Figure 4c, which shows the clay content at the depth of 100–200 cm, identifies a slight decrease in pixels with high amounts of clay in relation to the 30–60 cm layer in ATBs and a noticeable increase in certain ECBs. In general, at country level, an average increase of less than 2% was
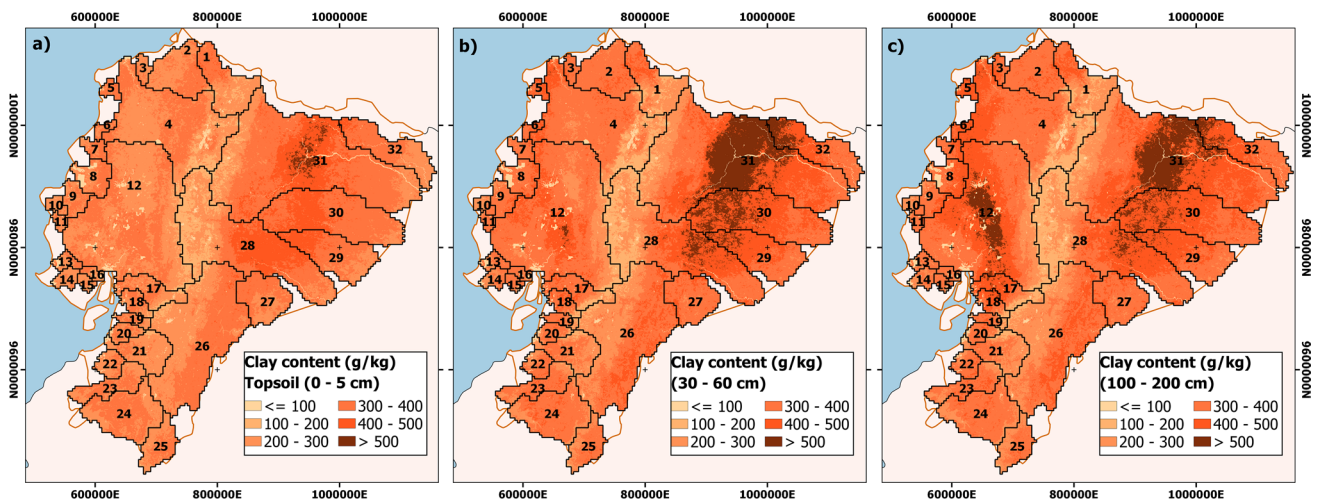
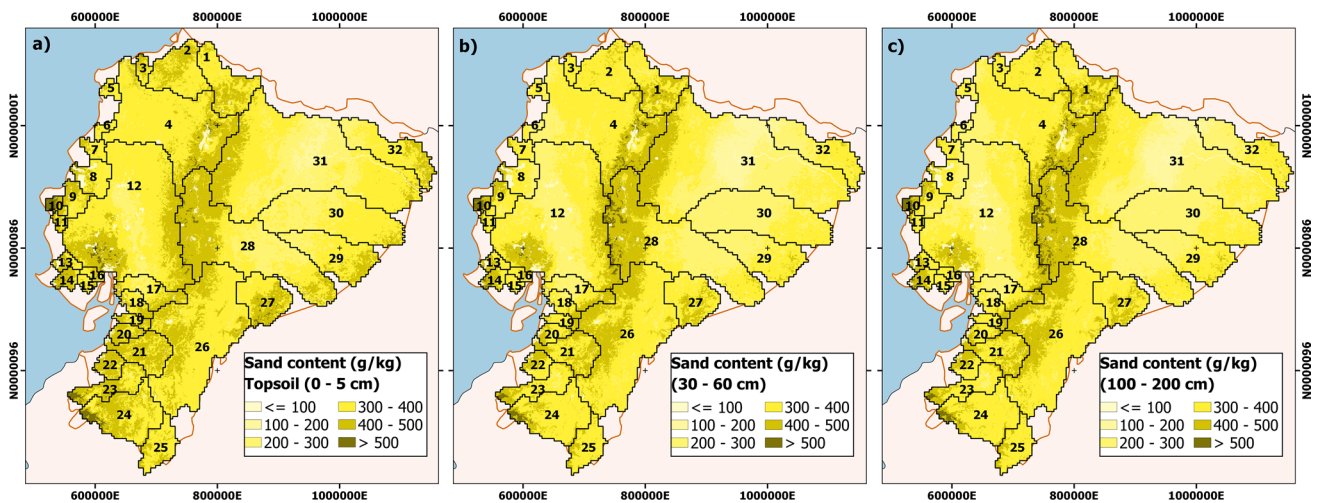**Fig. 4** Comparison of clay spatial distribution in Ecuadorian basins (g/kg)

Fig. 5 Comparison of sand spatial distribution in Ecuadorian basins (g/kg)

recorded between depths of 30–60 and 100–200 cm. Clay concentrations spatial distribution of at pixel level ranged from 0 to 722 g/kg, with an average value of 361.69 g/kg. At basins level, its spatial distribution was the same as in the two previous depths (maximum and minimum concentration values), with 440.58 g/kg in ATB Conocoto-Curaray (Id 30 in Fig. 4c and Supplementary data) and 278.04 g/kg in ECB Jubones (Id 21 in Fig. 4c and Supplementary data). At this depth, the increase in clay concentration in ECB Guayas stands out (Id 12 in Fig. 4c and Supplementary data), which went from 275.98 g/kg in topsoil to 381.41 g/kg in 100–200 cm layer, registering the greatest modification of clay content at basin level, reaching almost 38% between these two depths mentioned, while the basin that presented the least modification was

ECB Mira (Id 1 in Fig. 4c and Supplementary data), with a value less than 4%.

Sand content

By analyzing topsoil (Fig. 5a), the greatest amount of sand is concentrated in the ECBs coastal strip, due to its proximity to Pacific Ocean. In areas near the Andes Mountains of ECBs Mira, Esmeraldas and Guayas (Id 1, 4 and 12 in Fig. 5a and Supplementary data, respectively) and ATB Pastaza (Id 28 in Fig. 5a and Supplementary data) as in the sectors near Peru of ATBs Santiago and Morona (Id 26 and 27 in Fig. 5a and Supplementary data, respectively), higher sand contents are also recorded, with values per pixel greater than 500 g/kg. At pixel level, sand contents varied between 0
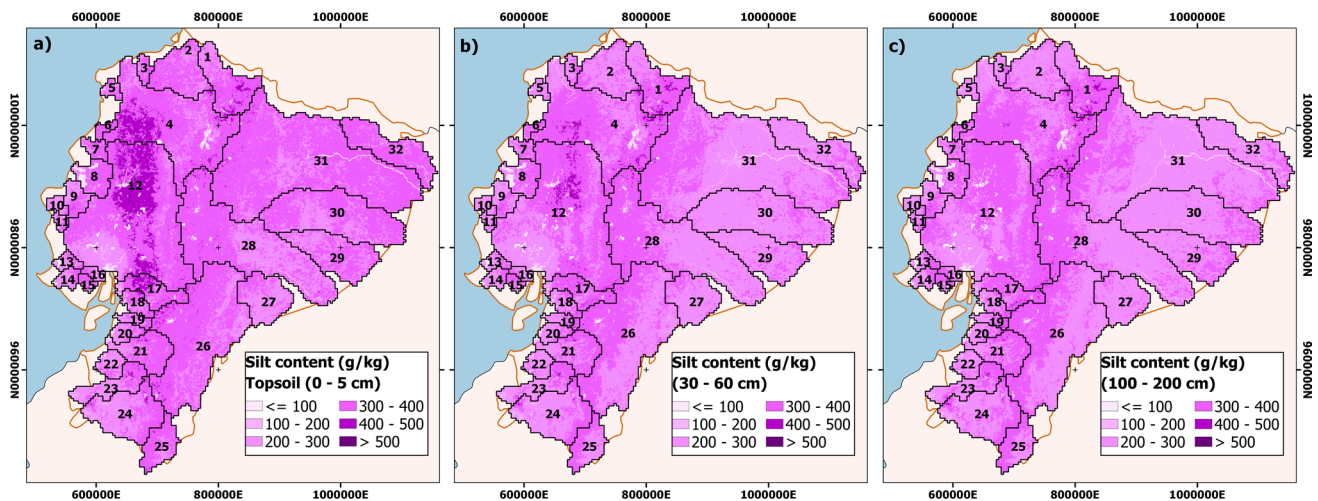
Fig. 6 Comparison of silt spatial distribution in Ecuadorian basins (g/kg)

and 713 g/kg with an average value of 356.22 g/kg. At basins level, ECB Caña (Id 10 in Fig. 5a and Supplementary data) is the one that registers the highest content, with 471.97 g/kg, while ATB Napo (Id 31 in Fig. 5a and Supplementary data) was the one that registered the lowest sand content, with 309.41 g/kg.

Analyzing depth 30–60 cm (Fig. 5b), a slight decrease in the sand content can be observed in all Ecuadorian basins in relation to topsoil. At pixel level, a maximum value of sand of 745 g/kg and 0 g/kg as a minimum value were recorded, with an average value of 333.04 g/kg. On average, 7% less sand was recorded in this profile compared to the previous one, even though some pixels appeared with values higher than those recorded in topsoil. The maximum value at basins level remained in ECB Caña (Id 10 in Fig. 5b and Supplementary data) with 452.73 g/kg, while in the minimum value a small displacement towards the north of the country was registered, being ATB Conocoto-Curaray (Id 30 in Fig. 5b and Supplementary data) which reported the lowest value (272.41 g/kg).

Through the analysis of Fig. 5c (100–200 cm), a slight decrease in relation to depth 30–60 cm (less than 0.6% average difference) is again identified. At pixel level, sand contents varied between 0 and 738 g/kg, with an average value of 331.08 g/kg. At basin level, maximum and minimum value was like the previous profile, with 450.64 g/kg for ECB Caña (Id 10 in Fig. 5c and Supplementary data) and 271.78 g/kg for ATB Conocoto-Curaray (Id 30 in Fig. 5c and Supplementary data).

Silt content

In Fig. 6a, silt content can be observed in topsoil. At pixel level, highest silt concentration is recorded in ECBs, especially in ECB Guayas (Id 12 in Fig. 6a), with a large presence of areas with silt contents greater than 500 g/kg. Values per pixel between 0 and 514 g/kg were recorded, with a mean value of 318.90 g/kg. At basin level, ECB Taura (Id 17 in Fig. 6a and Supplementary data) is the one that registers the highest silt content, with 352.87 g/kg, while ECB Javite (Id 13 in Fig. 6a and Supplementary data) recorded the least amount of silt, with 242.31 g/kg.

For depth 30–60 cm, Fig. 6b shows a decrease in silt content for all Ecuadorian basins (approximately 8% less concentration relative to topsoil). At pixel level, higher values were recorded in relation to topsoil, reaching a maximum value of 518 g/kg (in almost all sections where values above 500 g/kg were previously recorded) and a mean value of 294.53 g/kg. At basin level, maximum and minimum values are recorded in the same ECBs of topsoil, Taura and Javite (Id 17 and 13 in Fig. 6b and Supplementary data) with 328.05 and 236.87 g/kg, respectively.

Analyzing the deepest profile (Fig. 6c), the tendency to decrease in silt content is maintained (although to a lesser extent in relation to the previous comparison) and, in relation to profile 30–60 cm, a decrease of less than 2% was recorded. At pixel level, the maximum value was 536 g/kg and its mean value reached 290.38 g/kg. These values have made it possible to identify that, despite the fact that in almost the entire study area a sustained decrease in silt content has been recorded as the pedological profile is deeper, ECB Mira (Id 1 in Fig. 6c) recorded several pixels with higher values as depth increased, while ECB Guayas (Id 12 in Fig. 6c), which previously recorded a sustained increase in the amount of silt in certain pixels of its territory, in this profile (100–200 cm) did not recorded no value higher than 480 g/kg. At basin level, ECB Mira (Id 1 in Fig. 6c and Supplementary data) now registers the highest values with
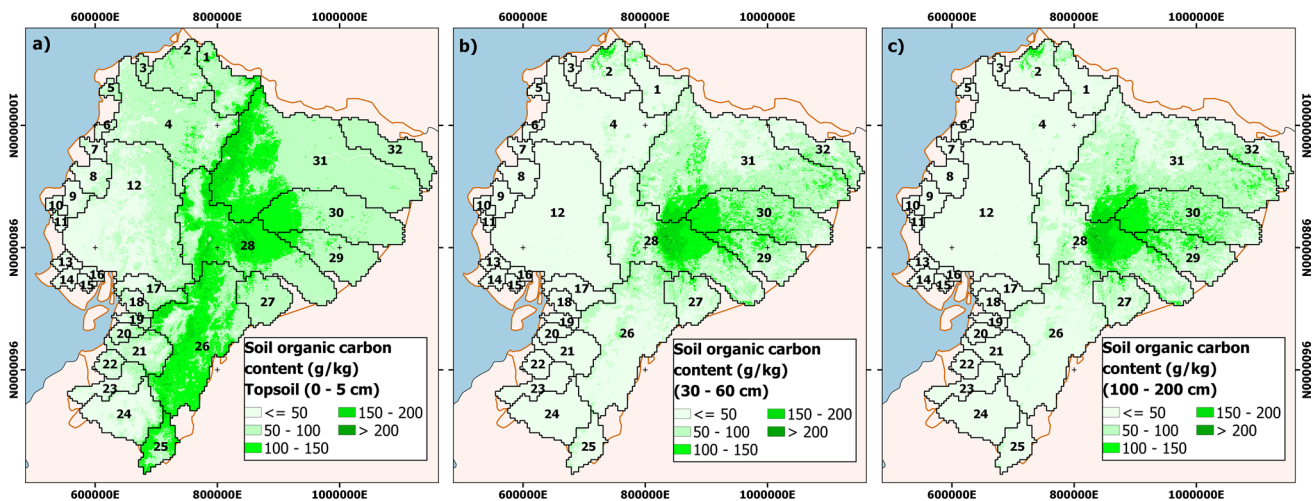
Fig. 7 Comparison of SOC spatial distribution in Ecuadorian basins (g/kg)

321.89 g/kg while ECB Javite (Id 13 in Fig. 6c and Supplementary data) still registers the lowest values at basin level, although this time its values are higher even when compared to topsoil (245.47 g/kg).

SOC content

By means of Fig. 7a, SOC contents in topsoil are analyzed. Highest values of organic matter are concentrated near the Andes Mountain in direction of ATBs, showing a behavior directly proportional to rainfall distribution, which is much greater in ATBs (Delgado et al. 2022) and that would have a direct impact on the growth vegetation cycle. At pixel level, maximum values of 232.30 g/kg and a mean value of 76.98 g/kg were recorded. At basin level, ATB Santiago (Id 26 in Fig. 7a and Supplementary data) is the one that registers the highest SOC content, with 111.94 g/kg, while ECB Zapotal (Id 14 in Fig. 7a and Supplementary data) was the one that registered the least amount of SOC with 29.72 g/kg.

Analyzing the 30–60 cm depth, Fig. 7b showed inferior results in almost the entire Ecuadorian territory, with an approximate decrease of 40% in relation to topsoil, even though, at pixel level, higher values were recorded (234.50 g /kg) in ATB Pastaza (Id 28 in Fig. 7b and Supplementary data). The average SOC content was 46.18 g/kg. At basin level, ATB Conocoto-Curaray (Id 30 in Fig. 7b and Supplementary data) was the one that registered the maximum SOC content, with 91.71 g/kg, while the ECB Daule (Id 15 in Fig. 7b and Supplementary data) recorded the minimum value of 12.44 g/kg.

Figure 7c, which represents a depth of 100–200 cm, showed very similar values to profile 30–60 cm (little perceptible visual changes), registering an average decrease of less than 8%. At pixel level, the maximum value was 227.70 g/kg while the average value was 42.83 g/kg. At basin level, ATB Conocoto-Curaray (Id 30 in Fig. 7c and Supplementary data) continues to record the maximum value (91.39 g/kg) while ECB Ayampe (Id 11 in Fig. 7c and Supplementary data) registered the minimum value of 10.26 g/kg. In general, SOC concentration in Ecuadorian basins decreased with increasing depth.

K-factor spatial distribution at different depths of the soil pedological profile

Because R-Factor mainly affects topsoil (Al Rammahi and Khassaf 2018), highest rainfall erosivity values are concentrated in this profile. This argument could be corroborated with Fig. 8a, which shows the K-Factor spatial distribution in topsoil of Ecuadorian basins. The regions most prone to soil erosion considering their erodibility are concentrated in ECB (especially in central-western part of the country) and in small sections of the northeastern part of the country. The values per pixel ranged from 0.03 to 0.12 t h/MJ mm, with an average value of 0.06 t h/MJ mm. Both at pixel and basin level, ECBs Taura and Guayas (Id 17 and 12 in Fig. 8a and Supplementary data in topsoil) recorded the highest values (values per pixel higher than 0.11 t h/ MJ mm and average values per basin higher than 0.064 t h/MJ mm). At basin level, lowest values reached 0.051 t h/MJ mm and were recorded in two ATBs (Morona and Conocoto-Curaray, Id 27 and 30 in Fig. 8a and Supplementary data) and one ECB (Caña, Id 10 in Fig. 8a and Supplementary data). Highest values of K-Factor coincide with the regions where silt content is higher. Likewise, in a large part where SOC content was high, K-Factor values decreased, even though some areas also shared high silt values. In relation to sand content, it was expected that the regions with high
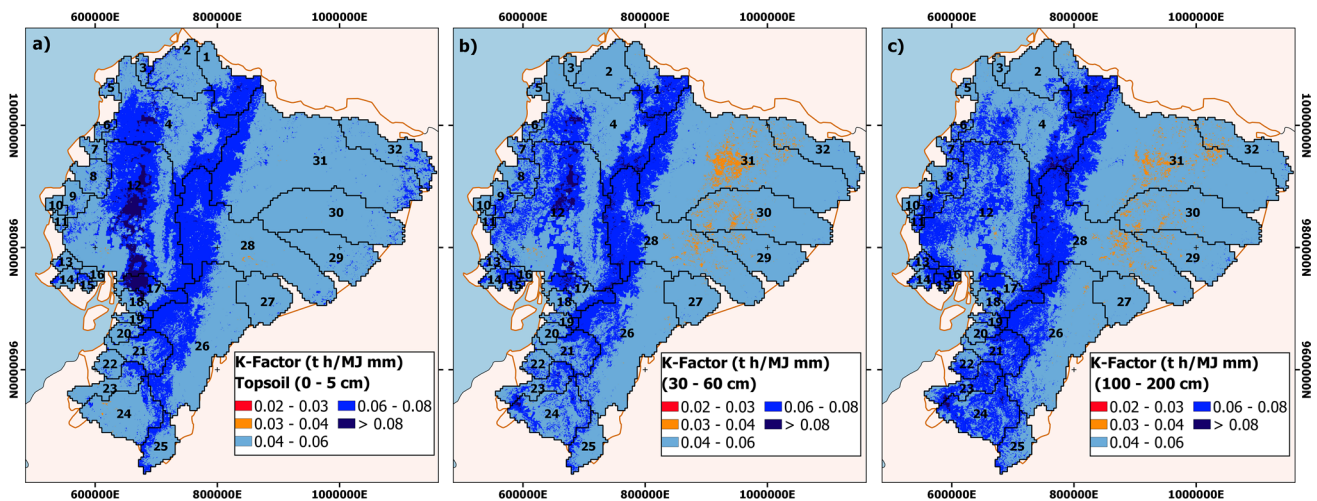
Fig. 8 K-Factor Spatial distribution (t h/MJ mm) at different depths of the soil pedological profile

contents would present lower K-Factor values (Al Rammahi and Khassaf 2018), but this condition was not fully met, possibly because high percentages of silt and low percentages of SOC predominated in these regions. With respect to clay, high contents of this soil type would mean a decrease in K-Factor (Al Rammahi and Khassaf 2018), a conclusion that could be corroborated in a large part of Ecuadorian territory. Higher clay concentrations were recorded in profiles 30–60 and 100–200 cm, especially in ATBs, where K-Factor values decreased even to almost 0.03 t h/MJ mm.

At pixel level, at depth of 30–60 cm (Fig. 8b), range of values was 0.032 and 0.117 t h/MJ mm, with an average value of 0.054 t h/MJ mm; while for 100–200 cm profile (Fig. 8c), the range was from 0.134 to 0.033 t h/MJ mm, with a mean value of 0.055 t h/MJ mm. A slight increase in K-Factor values can be observed in 100–200 cm profile in relation to 30–60 cm. This behavior can be associated with the fact that SOC content decreased while silt content remained almost unchanged (the latter registered a change of less than 2%).

Discussion

Soil properties differences according to the pedological profile

An increase or decrease in clay, sand, silt and SOC content has a direct impact on the behavior of the soil profile against rainfall erosion. Each of these components plays a different and fundamental role depending on its proportion at pixel level in Ecuadorian territory.

Considering the percentage distribution in Fig. 9, the soil characteristics that predominated in their erodibility in

Ecuadorian basins were clay and silt (in order of relevance, respectively). Although the changes between all the depths were not so marked, a low clay content together with a high silt content were the cause of generating the highest values of K-Factor and were recorded in topsoil. At this depth, lowest percentage clay content was recorded (30.80%), while the percentage silt content was the highest (30.20%).

30–60 cm depth was the one that recorded the best K-Factor values, where the highest clay percentage concentration was recorded in relation to the two remaining depths, reaching 40.13%, while the percentage content of silt was the lowest (26.43%).

Depth 100–200 cm recorded average K-Factor values very similar to topsoil, although its spatial distribution was more regular (in topsoil the highest values were concentrated in smaller regions, which could cause major erosion problems in those specific areas). In profile 100–200 cm it is observed that, although silt percentage content was lower than 30–60 cm profile (0.34% less), clay content was also slightly lower (0.10% less), which resulted in an average increase of 0.001 t h/MJ mm in K-Factor.

SOC content, despite being a very important soil characteristic, did not mean a great variation in the K-Factor generation, which is associated with the low concentration registered in Ecuadorian territory.

Relationship of K-factor and environmental parameters

K-factor results did not present significant variations in relation to the depth of analysis, which means that the contents of clay, silt, sand and SOC did not vary significantly between these soil depth profiles.
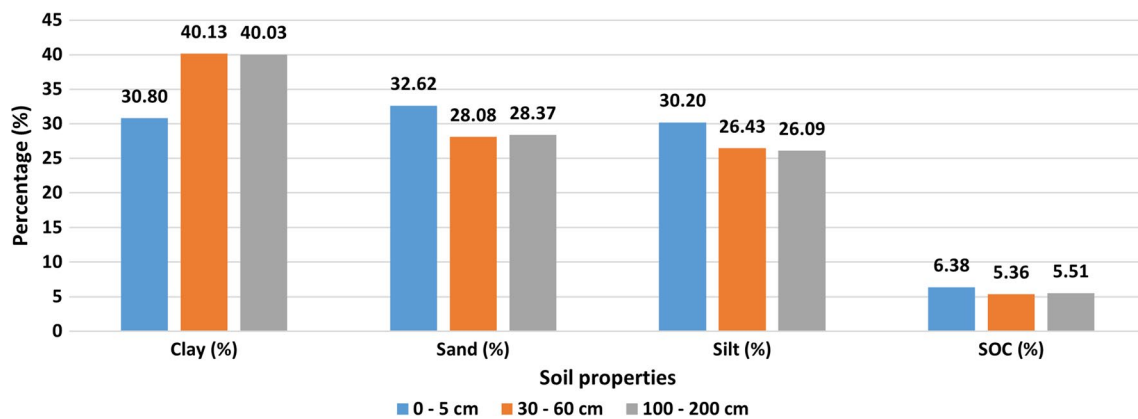
Fig. 9 Soil characteristics percentage distribution at soil depth (pixel scale). Each color represents a depth of the soil analyzed

When comparing K-Factor results with elevation ranges (Fig. 10a) for all depths, highest median values were recorded at elevations above 3000 m (approximately 0.067 t h/MJ mm in all depths) but higher scattered values are recorded in the deeper profile (100–200 cm, Fig. 10a3). Analyzing the K-Factor, lowest median values in topsoil (Fig. 10a1) were recorded in elevation range of 600–900 m (0.051 t h/MJ mm), with very small differences with the ranges 300–600 m (0.0515 t h/MJ mm) and 900–1600 m (0.052 t h/MJ mm). While for profiles 30–60 cm and 100–200 cm (Fig. 10a2, a3), lowest median values were recorded in the range of 300–600 m (0.046 t h/MJ mm) with very marked differences in relation to other elevation ranges. In general, elevations (excluding the 0–300 m range) have a directly proportional incidence on K-Factor values. That is, at higher elevations, K-Factor values are higher and vice versa. This behavior can be seen more clearly in 30–60 and 100–200 cm profiles (Fig. 10a2 and a3).

When considering Land Cover (Fig. 10b), there are very marked differences in topsoil (Fig. 10b1) in relation to the 2 deeper profiles, because the incidence of land cover decreases as the depth of analysis increases. Within topsoil, "Crop" stands out as the most damaging type according to erodibility, generating the highest K-Factor values (Fig. 10b1). In this category, even though "Crop" presents average values very similar to "Grass" (0.066 versus 0.065 t h/MJ mm), the data concentration area is clearly much higher in "Crop", reaching values of up to 0.078 t h/MJ mm, which is considered an important difference given the low variability between land covers. Analyzing the best land cover related to soil erodibility, "Forest" is the one that presents the best conditions in all the analysis profiles, with average values very close to 0.05 t h/MJ mm (Fig. 10b1, b2 and b3). Regarding the highest values for 30–60 and 100–200 cm depths, Fig. 10b2 and b3), "Grass" was the one that presented the most unfavorable conditions for soil

erodibility, with values like what "Crop" represented in topsoil, 0.066 t h/MJ mm.

In general, these results allow us to identify that "Forest" transmits a protective effect that counteracts the soil erodibility problems and with these the R-Factor effects (Arifeen and Chaudhry 1998; Delgado et al. 2022). On the contrary, "Crop" is considered one of the most damaging covers for soil erosion and its erodibility (Brunel and Seguel 2011), which is reflected in the high values of K-Factor, especially in topsoil. As for "Grass", even though this land cover reduces surface runoff, its main function is to regulate SOC values instead of acting against erosive forces (Zheng et al. 2021), therefore, also considering the low percentages of SOC in all Ecuadorian basins, "Grass" also registered part of the highest median K-Factor values in Ecuadorian territory.

Sources of uncertainty, spatial resolution and research limitations

Williams equation (Williams 1995), a worldwide applied methodology (Al Rammahi and Khassaf 2018; Jiang et al. 2020; Kolli et al. 2021; Guduru and Jilo 2022) allows to analyze soil erodibility at pixel scale, without the need to distribute the Ecuadorian territory by soil types such as those presented by the FAO through the Digital Soil Map of the World (DSMW) (https://www.fao.org/land-water/land/land-governance/land-resources-planning-toolbox/category/details/en/c/1026564/), which groups several strips of land based on the concentration of each soil type, generating a less real soil representation composition by generalizing larger areas through average values. Williams (1995) allows to classify on a finer scale the soil properties corresponding to clay, sand, silt and SOC, obtaining much more detailed results that allow better description of how the soil erodibility would act in the Ecuadorian territory. Despite this, this methodology, unlike other investigations (Chatterjee et al. 2014; Saha et al. 2022; Yang et al. 2022a, b) does
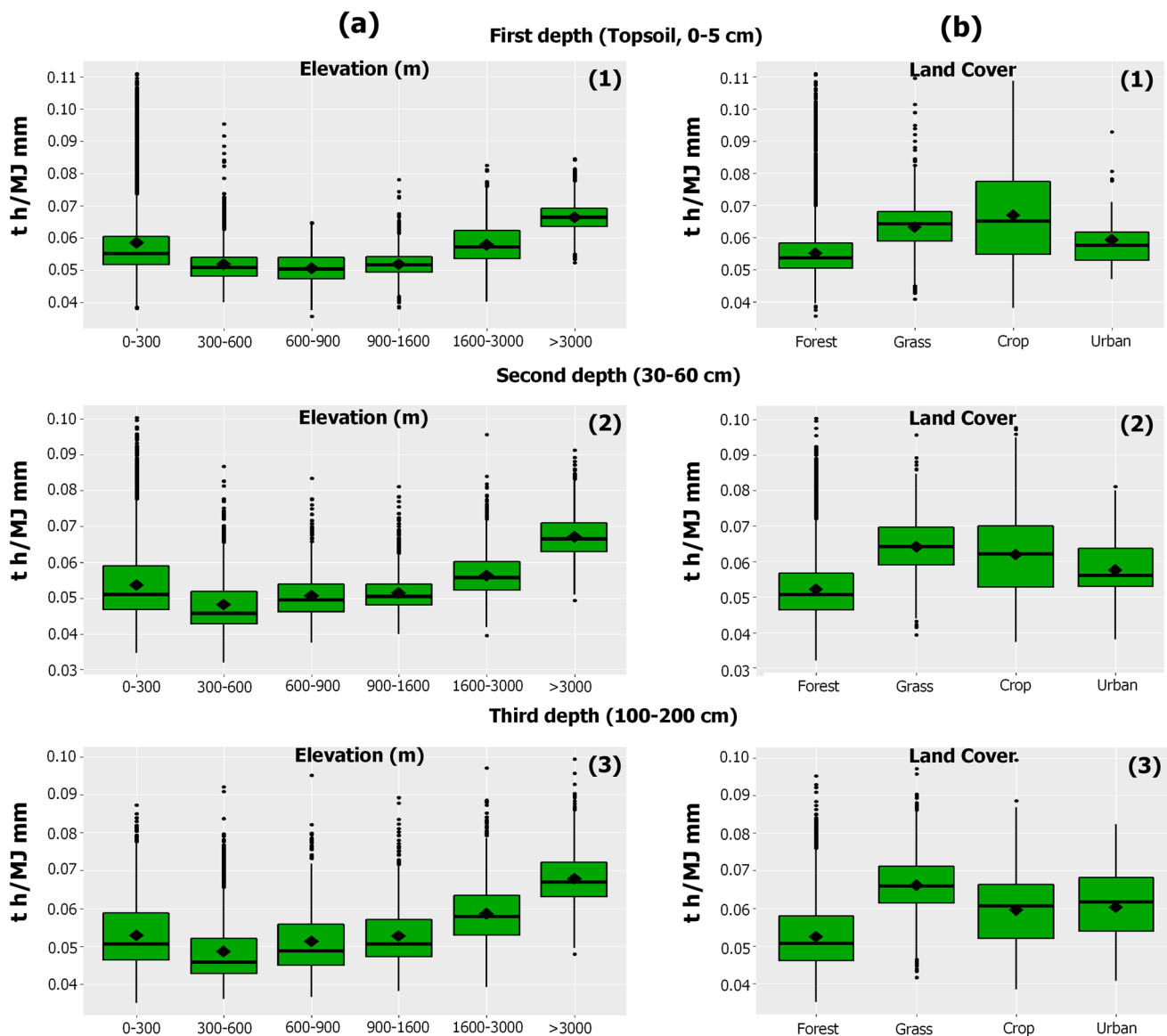
Fig. 10 Box plots of K-Factor values by analyzing of environmental parameters of elevation **a** and land cover (**b**) by depth. X-axis label presents variables for category

not consider the "soil structure class" and the "soil profile permeability class" as independent elements, that can be considered a limitation but that are included (although in a general way) within the complementary equations (Eqs. 3, 4, 5 and 6), being able to partially generalize the Soil erodibility nomograph (Wischmeier and Smith 1978) that is commonly applies to obtain these results in each region of the world in particular.

Regarding investigation detail, taking the spatial resolution of 100×100 m as a reference, it is considered highly reliable and precise, generating optimal results that can be coupled to any other spatial resolution (especially coarser resolutions) and also allow a very detailed individual study by basins to be carried out, facilitating the generation of

control and mitigation measures to deal with possible erosion problems related to soil erodibility.

Additionally, at a pixel scale, it can be clearly seen how the topsoil presents more unfavorable results for eventual soil erosion calculated by applying the RUSLE, followed by the 100–200 cm profile and, finally, as the most favorable profile, the intermediate depth 30–60 cm (Fig. 11 per pixel). However, if the analysis is carried out on an average scale by basins, the results generate a certain dispersion, due to the average and rounding generated by the cut of pixels that causes the delimitation of each basin and because the range of values is very low (between 0.03 and 0.12 t h/ MJ mm). Through this analysis by basin, the deepest profile (100–200 cm) is identified as the layer most prone to erosion

Fig. 11 Histogram shows K-Factor mean distribution at the depth level of soil analysis. Each color represents the spatial level analyzed
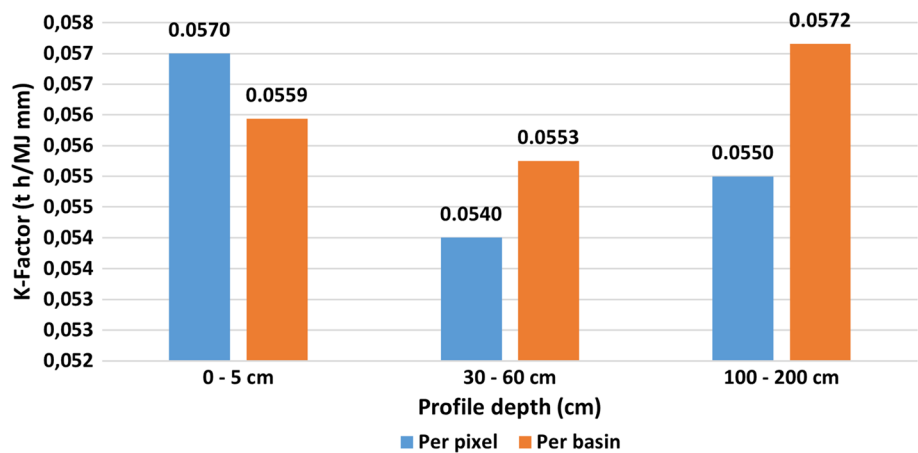
problems, with an average K-Factor of 0.057 t h/MJ mm (Fig. 11 per basin). Likewise, the second most unfavorable profile would be the topsoil with an average K-Factor of 0.056 t h/MJ mm (Fig. 11 per basin). Lastly, and similarly to the pixel analysis, intermediate layer is the one that presents the best results against soil erosion, with an average K-Factor of 0.055 t h/ MJ mm (Fig. 11 per basin). The average changes between the 3 pedological profiles were minimal.

Regarding analysis level, it is recommended that, for cases where K-Factor values register very small numerical ranges in study territory, consider the weighting at pixel level (without considering a territorial unit), because a basins level or by another unit of analysis much larger than the pixel extension would generate biases and dispersion of the real results, causing inconveniences in their interpretation.

The uncertainties, scope and limitations analyzed in this paragraph are not considered harmfully relevant in the application of this methodology on a national scale, but it is recommended to implement improvements in the future, applying national or regional classifications and methodologies that allow the generation of better approximations.

Conclusions

Soil erodibility spatial distribution at different pedological depths (0–5 cm, 30–60 cm, 100–200 cm) were modeled with information on soil characteristics obtained from Soil-Grids database for the first time at national scale in Ecuador. K-Factor values at pixel level showed great variability between the ECB and ATB, considering that the range of values was very low (0.03–0.12 t h/MJ mm on average). Average values of the profiles analyzed by basin groups were slightly higher in the ECBs (0.058 t h/MJ mm) in relation to the ATBs (0.052 t h/MJ mm). Clay and silt were the most relevant soil characteristics in K-Factor generation, while the low concentration of SOC did not allow this component to trigger its magnitudes. The qualitative analysis of

the environmental parameters made it possible to determine that the soils with the greatest erodibility problems are in the highest areas and are made up of "Crop" and "Grass" land covers. An average analysis per pixel allowed to determine that the pedological depth most prone to erodibility problems was topsoil (0.06 t h/MJ mm) while the intermediate depth (30–60 cm) registered slightly more favorable results (0.054 t h/ MJ mm) relative to the deepest layer (100–200 cm, 0.055 t h/MJ mm). Results of this research provide important information for the comprehensive management and sustainable soil use an erodibility approach, generating spatial models that can be applied to equations to determine soil loss at any depth, contributing to natural resources conservation programs, agricultural protection, disaster prevention and other applications in Ecuador.

Author contributions All the authors contributed equally in the different stages of the development of the research and in the writing of the manuscript that is submitted for evaluation.

Data availability Data will be made available on request.

Declarations

Conflict of interest The authors declare no competing interests.

References

Al Rammahi AHJ, Khassaf SI (2018) Estimation of soil erodibility factor in RUSLE equation for Euphrates River watershed using GIS. GEOMATE Journal 14(46):164–169

Amundson R, Berhe AA, Hopmans JW, Olson C, Sztein AE, Sparks DL (2015) Soil and human security in the 21st century. Science 348(6235):1261071

Arifeen SZ, Chaudhry AK (1998) Effect of different land uses on surface runoff and sediment yield in moist temperate zone. Pak J 48(1–4):97–101

Bahri H, Raclot D, Barbouchi M, Lagacherie P, Annabi M (2022) Mapping soil organic carbon stocks in Tunisian topsoils. Geoderma Reg 30:e00561

Bastola S, Dialynas YG, Bras RL, Noto LV, Istanbulluoglu E (2018) The role of vegetation on gully erosion stabilization at a severely degraded landscape: a case study from Calhoun Experimental Critical Zone Observatory. Geomorphology 308:25–39

Bonilla CA, Johnson OI (2012) Soil erodibility mapping and its correlation with soil properties in Central Chile. Geoderma 189:116–123

Brunel N, Seguel O (2011) Efectos de la erosión en las propiedades del suelo. Agro Sur 39(1):1–12

Cassol, E. A., Silva, T. S. D., Eltz, F. L. F., & Levien, R. (2018). Soil erodibility under natural rainfall conditions as the K factor of the universal soil loss equation and application of the nomograph for a subtropical Ultisol. Revista Brasileira de Ciência do Solo, 42.

Chatterjee S, Krishna AP, Sharma AP (2014) Geospatial assessment of soil erosion vulnerability at watershed level in some sections of the Upper Subarnarekha river basin, Jharkhand. India Environment Earth Sci 71(1):357–374. https://doi.org/10.1007/s12665-013-2439-3

Delgado D, Sadaoui M, Ludwig W, Méndez W (2022) Spatio-temporal assessment of rainfall erosivity in Ecuador based on RUSLE using satellite-based high frequency GPM-IMERG precipitation data. CATENA 219:106597

Delgado, D., Sadaoui, M., Pacheco, H., Méndez, W., & Ludwig, W. (2021). Interrelations Between Soil Erosion Conditioning Factors in Basins of Ecuador: Contributions to the Spatial Model Construction. In International Conference on Water Energy Food and Sustainability (pp. 892–903). Springer, Cham.

Elnashar A, Zeng H, Wu B, Fenta AA, Nabil M, Duerler R (2021) Soil erosion assessment in the Blue Nile Basin driven by a novel RUSLE-GEE framework. Sci Total Environ 793:148466

FAO. 2020. Global Forest Assessment 2010: Main Report. Food and Agriculture Organization of the United Nations (FAO) Forestry Paper 163, Rome. [www.fao.org/forestry/fra/en/; accessed: verified October 2022]

Goldman, S. J., & Jackson, K. E. (1986). Erosion and sediment control handbook.

Guduru, J. U., & Jilo, N. B. (2022). Assessment of rainfall-induced soil erosion rate and severity analysis for prioritization of conservation measures using RUSLE and Multi-Criteria Evaluations Technique at Gidabo watershed, Rift Valley Basin, Ethiopia. Ecohydrology & Hydrobiology.

Gürtekin E, Gökçe O (2021) Estimation of erosion risk of Harebakayiş sub-watershed, Elazig, Turkey, using GIS based RUSLE model. Environ Challeng 5:100315

Huang S, Eisner S, Haddeland I, Mengistu ZT (2022) Evaluation of two new-generation global soil databases for macro-scale hydrological modelling in Norway. J Hydrol 610:127895

Jiang Q, Zhou P, Liao C, Liu Y, Liu F (2020) Spatial pattern of soil erodibility factor (K) as affected by ecological restoration in a typical degraded watershed of central China. Sci Total Environ 749:141609

Kolli MK, Opp C, Groll M (2021) Estimation of soil erosion and sediment yield concentration across the Kolleru Lake catchment using GIS. Environ Earth Sci 80(4):1–14. https://doi.org/10.1007/s12665-021-09443-7

Krpec P, Horáček M, Šarapatka B (2020) A comparison of the use of local legacy soil data and global datasets for hydrological modelling a small-scale watershed: Implications for nitrate loading estimation. Geoderma 377:114575

Mhangara P, Kakembo V, Lim KJ (2012) Soil erosion risk assessment of the Keiskamma catchment, South Africa using GIS and remote sensing. Environ Earth Sci 65(7):2087–2102. https://doi.org/10.1007/s12665-011-1190-x

Musa, J. J., Anijofor, S. C., Obasa, P., & Avwevuruvwe, J. J. (2017). Effects of soil physical properties on erodibility and infiltration parameters of selected areas in Gidan Kwano.

Neitsch, S. L., Arnold, J. G., Kiniry, J. R., & Williams, J. R. (2000). Erosion Soil and Water Assessment Tool Theoretical Documentation Texas Agricultural Eksperiment Station.

Ochoa-Cueva P, Fries A, Montesinos P, Rodríguez-Díaz JA, Boll J (2013) Spatial estimation of soil erosion risk by land-cover change in the Andes of southern Ecuador. Land Degrad Dev 26(6):565–573

Ochoa PAA, Fries A, Mejía D, Burneo JI, Ruíz-Sinoga JD, Cerdà A (2016) Effects of climate, land cover and topography on soil erosion risk in a semiarid basin of the Andes. CATENA 140:31–42

Pacheco HA, Méndez W, Moro A (2019) Soil erosion risk zoning in the Ecuadorian coastal region using geo-technological tools. Earth Sci Res J 23(4):293–302

Prasannakumar V, Shiny R, Geetha N, Vijith HJEES (2011) Spatial prediction of soil erosion risk by remote sensing, GIS and RUSLE approach: a case study of Siruvani river watershed in Attapady valley, Kerala. India Environ Earth Sci 64(4):965–972. https://doi.org/10.1007/s12665-011-0913-3

Rehman, M. A., Desa, S. M., Abd Rahman, N., Mohd, M. S. F., Aminuddin, N. A. S., Taib, A. M., ... & Mohtar, W. H. M. W. (2022). Correlation between soil erodibility and light penetrometer blows: A case study in Sungai Langat, Malaysia. Physics and Chemistry of the Earth, Parts A/B/C, 103262.

Renard, K. G., Foster, G. R., Weesies, G. A., McCool, D. K., & Yoder, D. C. (1996). Predicting soil erosion by water: A guide to conservation planning with the Revised Universal Soil Loss Equation (RUSLE). Agriculture handbook, 703.

Riquetti NB, Mello CR, Leandro D, Guzman JA, Beskow S (2022) Assessment of the soil-erosion-sediment for sustainable development of South America. J Environ Manag 321:115933

Saha M, Sauda SS, Real HRK, Mahmud M (2022) Estimation of annual rate and spatial distribution of soil erosion in the Jamuna basin using RUSLE model: A geospatial approach. Environ Challeng 8:100524

Tang J, Liu G, Xie Y, Dun X, Wang D, Zhang S (2021) Ephemeral gullies caused by snowmelt: A ten-year study in northeastern China. Soil Tillage Res 212:105048

Wang H, Zhang G, Liu F, Geng R, Wang L (2017) Effects of biological crust coverage on soil hydraulic properties for the Loess Plateau of China. Hydrol Process 31(19):3396–3406

Wei L, Liu Y, Routh J, Tang J, Liu G, Liu L, Zhang H (2019) Release of heavy metals and metalloids from two contaminated soils to surface runoff in southern China: a simulated-rainfall experiment. Water 11(7):1339

Williams, J.R. (1995). Chapter 25. The EPIC Model. p. 909–1000. In Computer Models of Watershed Hydrology. Water Resources Publications. Highlands Ranch, CO.

Wischmeier WH, Mannering JV (1969) Relation of soil properties to its erodibility. Soil Sci Soc Am J 33(1):131–137

Wischmeier, W. H., & Smith, D. D. (1978). Predicting rainfall erosion losses: a guide to conservation planning (No. 537). Department of Agriculture, Science and Education Administration.

Yang, M., Yang, Q., Zhang, K., Wang, C., Pang, G., & Li, Y. (2022a). Effects of soil rock fragment content on the USLE-K factor estimating and its influencing factors. International Soil and Water Conservation Research.

Yang X, Leys J, Gray J, Zhang M (2022b) Hillslope erosion improvement targets: Towards sustainable land management across New South Wales. Australia CATENA 211:105956

Yin J, Gentine P, Zhou S, Sullivan SC, Wang R, Zhang Y, Guo S (2018) Large increase in global storm runoff extremes driven by climate and anthropogenic changes. Nat Commun 9(1):1–10

Zheng, J. Y., Zhao, J. S., Shi, Z. H., & Wang, L. (2021). Soil aggregates are key factors that regulate erosion-related carbon loss in citrus orchards of southern China: Bare land vs. grass-covered land. Agric Ecosyst Environ, 309, 107254.